Radiative production of sneutrinos in e^+e^- annihilation with polarized beams

F. Franke and H. Fraas
Physikalisches Institut, Universität Würzburg, D-97074 Würzburg, Federal Republic of Germany
(Received 12 February 1993; revised manuscript received 18 June 1993)

We give for the process $e^+ + e^- \to \tilde{\nu} + \bar{\tilde{\nu}} + \gamma$ of radiative sneutrino production with polarized beams the complete analytic expression for the transition amplitude. For beam energies between 100 and 500 GeV the total cross section, the photon energy spectrum, and photon angular distribution as well as the respective longitudinal polarization asymmetries are computed in representative gaugino-Higgsino mixing scenarios with the sneutrino decaying only into the lightest neutralino. Comparing the results with those for the competing standard process of radiative neutrino production we show that with the expected luminosity for a 500-GeV e^+e^- collider it would be difficult to identify a sneutrino lighter than both the chargino and the second lightest neutralino. The use of longitudinally polarized beams especially would not facilitate identification of the sneutrino in this mass region.

PACS number(s): 14.80.Ly, 13.10.+q, 13.88.+e

I. INTRODUCTION

Despite the extraordinary success of the standard model (SM) and the lack of experimental evidence for supersymmetric particles at the present e^+e^- colliders, especially at the CERN e^+e^- collider LEP 100, it is widely believed that the SM is not a fundamental description of nature and the ideal of supersymmetry (SUSY) remains the favorite candidate for a possible solution of some of its problems. Recent LEP data concerning the extrapolation of the coupling constants to grand unified theory (GUT) energies [1] even provide a new motivation for studying supersymmetric phenomena. Therefore, the search for supersymmetric particles is still on the program at present and future accelerators.

Pair production $e^+ + e^- \to \tilde{\nu} + \bar{\tilde{\nu}}$ of the scalar supersymmetric partners of the standard neutrinos has been extensively discussed for polarized beams by Chiappetta *et al.* [2] and by Wendel and Fraas [3]. Assuming the lightest neutralino to be the lightest supersymmetric particle (LSP), reasonable decay rates into charginos $\tilde{\nu} \to e^- + \tilde{\chi}_i^+$ $(i=1,2)$ or into one of the heavier neutralinos $\tilde{\nu} \to \nu + \chi_i^0$ $(i=2,3,4)$ are crucial for detecting sneutrinos. These decays leading to characteristic events with a lepton pair or hadronic jets plus missing energy [4,5] are allowed for the supersymmetric parameters M and μ confined to the region $M \le (1-2)m_{\tilde{\nu}}$ or $-m_{\tilde{\nu}} \le \mu \le (1-2)m_{\tilde{\nu}}$ [6]. If, however, the sneutrino is lighter than both the light chargino $\tilde{\chi}_1^+$ and the second lightest neutralino $\tilde{\chi}_2^0$, the only way to identify sneutrino production in e^+e^- annihilation is via the bremsstrahlung photon in the radiative process $e^+ + e^0 \to \tilde{\nu} + \bar{\tilde{\nu}} + \gamma$.

For beam energies up to 100 GeV, this process has been discussed by Chiappetta *et al.* [7] under the aspect that the sneutrino is the LSP, being stable and invisible. The results of LEP experiments together with astrophysical bounds, however, rule out this possibility [8]. Further, Chiappetta *et al.* restricted themselves to the special case where the light chargino is a pure W-ino.

In this paper we study in the energy region between 100- and 500-GeV radiative production of an otherwise invisible sneutrino with polarized beams for four scenarios with different gaugino-Higgsino mixing and sneutrino mass. The signature of a single photon accompanied by no other detectable particles is the same as for the radiative production of neutrino pairs $e^+ + e^- \to \nu + \bar{\nu} + \gamma$; therefore, this standard process is the source of the most substantial background [9]. Vice versa, radiative sneutrino production could represent a background process for neutrino counting experiments.

Since for the processes $e^+ + e^- \to \tilde{\nu} + \bar{\tilde{\nu}}$ and $e^+ + e^- \to \nu + \bar{\nu}$ the polarization asymmetries show significant differences [2] one would expect also here that experiments with suitably polarized beams would be helpful to discriminate between the supersymmetric process and the standard neutrino background.

As for $e^+ + e^- \to \tilde{\nu} + \bar{\tilde{\nu}}$ it is especially the production of electron sneutrinos $\tilde{\nu}_e$ via Z^0 exchange and exchange of charginos $\tilde{\chi}_i^+$ $(i=1,2)$, which, because of the chiral structure of the chargino couplings, is expected to show a strong dependence on the beam polarization, significantly different from that of the standard process.

Since the chargino couplings are functions of the W-ino–charged-Higgsino mixings one also expects at high energies, i.e., in some distance from the Z^0 peak, considerable variations of cross sections and polarization asymmetries with different mixing scenarios.

For $\tilde{\nu}_\mu$ and $\tilde{\nu}_\tau$ production the reaction only proceeds via Z^0 exchange. Therefore at high energies $\tilde{\nu}_e$ production, on the one hand, and $\tilde{\nu}_\mu$ or $\tilde{\nu}_\tau$ production, on the other hand, should show a rather different behavior; at energies far beyond the Z^0 region the latter ones are significantly suppressed. So we restrict ourselves mostly to the discussion of the production of electron sneutrinos.

Within the framework of the minimal supersymmetric extension of the standard model (MSSM) [10] we present in Sec. II the Feynman amplitudes of $e^+ + e^- \to \tilde{\nu}_e + \bar{\tilde{\nu}}_e + \gamma$ for general chargino mixing and some for-

mulas for the transition probability, the three-particle phase space and for polarization asymmetries. Section III contains the numerical results for the total cross section, the photon energy spectrum, and the photon angular distribution including a discussion of the background from radiative neutrino production.

In the Appendix we list the complete analytic expressions for the transition probability with polarized beams together with our notation and conventions for the description of beam polarizations.

II. FEYNMAN AMPLITUDES, CROSS SECTIONS, AND POLARIZATION ASYMMETRIES

The Feynman graphs contributing to the process $e^+ + e^- \to \tilde{\nu}_e + \bar{\tilde{\nu}}_e + \gamma$ are shown in Fig. 1. The relevant couplings of the supersymmetric particles can be deduced from the following interaction Lagrangians of the minimal supersymmetric extension of the standard model (as for notations and conventions, we closely follow [10]):

$$\mathcal{L}_{\tilde{\nu}\bar{\tilde{\nu}}Z} = \frac{-ig}{2\cos\theta_W} Z_\mu \tilde{\nu}^* \overleftrightarrow{\partial^\mu} \tilde{\nu} \ , \tag{1}$$

$$\mathcal{L}_{e\tilde{\nu}_e\tilde{\chi}_j} = -g \sum_{j=1}^{2} (V_{j1}^* \bar{\tilde{\chi}}_j^{+C} P_L e \tilde{\nu}_e^* + V_{j1} \bar{e} P_R \tilde{\chi}_j^{+C} \tilde{\nu}_e) \ , \tag{2}$$

$$\mathcal{L}_{\tilde{\chi}_j\tilde{\chi}_j\gamma} = -e A_\mu \bar{\tilde{\chi}}_j^{+} \gamma^\mu \tilde{\chi}_j^{+} \ . \tag{3}$$

For completeness, we add the Lagrangian for the $Z^0 e^+ e^-$ coupling:

$$\mathcal{L}_{eeZ} = \frac{-g}{\cos\theta_W} Z_\mu \bar{e} \gamma^\mu (L P_L + R P_R) e \tag{4}$$

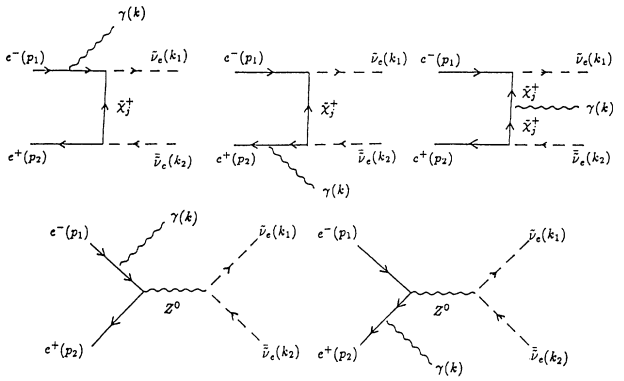

FIG. 1. Feynman graphs for $e^+e^- \to \tilde{\nu}_e \bar{\tilde{\nu}}_e \gamma$. In the case of $\tilde{\nu}_{\mu,\tau}$ production, only Z^0 exchange contributes to the process.

with

$$L = -\tfrac{1}{2} + \sin^2\theta_W \ , \quad R = \sin^2\theta_W \ . \tag{5}$$

In Eqs. (1)–(4), $\tilde{\chi}_j^+$ $(j=1,2)$ and e are the four-component spinors of the charginos and the electron, while $\tilde{\nu}$ is the field of the sneutrino; $\tilde{\chi}_j^{+C}$ are charge-conjugated spinor fields. Furthermore, $P_{R,L} = (1 \pm \gamma_5)/2$ denote the right- and left-handed projection operators, $g = e/\sin\theta_W$ $(e>0)$, and V_{ij} is the 2×2 unitary matrix appearing in the diagonalization of the W-ino–charged-Higgsino mass matrix (see [11] for more details). Notice that in [10] the light chargino was called $\tilde{\chi}_2^\pm$ instead of $\tilde{\chi}_1^\pm$ in [11] and here.

With these Lagrangians the Feynman amplitudes for chargino exchange read

$$\mathcal{M}_1 = ieg^2 \sum_{j=1}^{2} |V_{j1}|^2 \frac{\bar{v}(p_2) P_R \not{k}_2 (\not{p}_1 - \not{k}) \not{\varepsilon} u(p_1)}{(2p_1 k)[(k_2 - p_2)^2 - m_{\tilde{\chi}_j^+}^2]} \ , \tag{6}$$

$$\mathcal{M}_2 = ieg^2 \sum_{j=1}^{2} |V_{j1}|^2 \frac{\bar{v}(p_2) \not{\varepsilon} (\not{p}_2 - \not{k}) P_R \not{k}_1 u(p_1)}{(2p_2 k)[(k_1 - p_2)^2 - m_{\tilde{\chi}_j^+}^2]} \ , \tag{7}$$

$$\mathcal{M}_3 = -ieg^2 \sum_{j=1}^{2} |V_{j1}|^2 \frac{\bar{v}(p_2) P_R (\not{k}_2 + m_{\tilde{\chi}_j^+}) \not{\varepsilon} (-\not{k}_1 + m_{\tilde{\chi}_j^+}) P_L u(p_1)}{[(k_2 - p_2)^2 - m_{\tilde{\chi}_j^+}^2][(k_1 - p_1)^2 - m_{\tilde{\chi}_j^+}^2]} \ , \tag{8}$$

and for Z^0 exchange we obtain

$$\mathcal{M}_4 = \frac{ieg^2}{2\cos^2\theta_W} \frac{\bar{v}(p_2)(\not{k}_1 - \not{k}_2) + (L P_L + R P_R)(\not{p}_1 - \not{k}) \not{\varepsilon} u(p_1)}{(2p_1 k)[(k_1 + k_2)^2 - m_Z^2 + i\Gamma_Z m_Z]} \ , \tag{9}$$

$$\mathcal{M}_5 = \frac{-ieg^2}{2\cos^2\theta_W} \frac{\bar{v}(p_2) \not{\varepsilon} (\not{p}_2 - \not{k}) (\not{k}_1 - \not{k}_2) (L P_L + R P_R) u(p_1)}{(2p_2 k)[(k_1 + k_2)^2 - m_Z^2 + i\Gamma_Z m_Z]} \ . \tag{10}$$

Here, $p_{1,2}$, $k_{1,2}$ and k denote the four-momenta of electron, positron, sneutrino, and antisneutrino, respectively, and ε^μ is the polarization vector of the photon.

From the total amplitude $\mathcal{M} = \sum_{i=1}^{5} \mathcal{M}_i$ and the spin density matrices in Eqs. (A4) and (A7) for electrons and positrons we obtain the transition probability $|\mathcal{T}_{fi}|^2$, summed over the photon polarizations:

$$\sum_{\text{phot pol}} |\mathcal{T}_{fi}|^2=[L^2(1-P_\parallel)(1+P'_\parallel)+R^2(1+P_\parallel)(1-P'_\parallel)]X_s$$
$$+(1-P_\parallel)(1+P'_\parallel)X_t+L(1-P_\parallel)(1+P'_\parallel)X_{st}+RLP_\perp P'_\perp X'_s+RP_\perp P'_\perp X'_{st} . \quad (11)$$

In Eq. (11), $P_\parallel$ ($P'_\parallel$) denotes the longitudinal polarization of the electron (positron) and $P_\perp$ ($P'_\perp$) is the degree of transverse polarization. The directions of the transverse polarizations, which are assumed to be parallel ($P_\perp P'_\perp>0$) are antiparallel ($P_\perp P'_\perp<0$) but otherwise arbitrary, have been absorbed in the coefficients X'_s and X'_{st}. X_s, X'_s, and X_t are contributions from Z^0 exchange and chargino exchange, respectively, and X_{st} and X'_{st} are interference terms. For the production of $\tilde{\nu}_\mu$ or $\tilde{\nu}_\tau$, it is $X_t=X_{st}=X'_{st}\equiv 0$, because in this case only Z^0 exchange contributes.

Since, independent of special scenarios discussed in the following section, the complete expressions for these coefficients may be useful for further investigations, we list them in the Appendix. Calculating these coefficients involves extensive algebra. We have therefore made use of the computer program FEYNCALC [12] (based on the computer language MATHEMATICA), which has been developed for calculations of Feynman amplitudes and trace evaluations.

Because of the chiral structure of the chargino-sneutrino couplings the contributions of the chargino exchange vanish for right-handed electrons and left-handed positrons ($P_\parallel=-P'_\parallel=+1$). For this polarization, production of sneutrinos of all three generations shows the same behavior which is significantly different from that of electron sneutrino production with unpolarized beams or a longitudinal polarization with $P_\parallel=-P'_\parallel=-1$. Since with increasing energy Z^0 exchange is more and more suppressed, $\tilde{\nu}_e$ production differs more from $\tilde{\nu}_\mu$ or $\tilde{\nu}_\tau$ production the higher the beam energy is.

Photon energy spectrum, photon angular distribution, and total cross section are computed by integrating the transition probability [Eq. (11)] over the respective domain of the three-particle phase space [13]:

$$dR_3=\frac{E^2}{8(2\pi)^5}dx\,dz\,d\cos\theta_\gamma d\phi_\gamma d\phi_{\tilde{\nu}} \quad (12)$$

with

$$\cos\theta_{\tilde{\nu}}=\frac{(2-x-z)^2-x^2-z^2}{2x(z^2-m^2_{\tilde{\nu}}/E^2)^{1/2}} . \quad (13)$$

Here, θ_γ is the angle between the photon and the electron beam and $\theta_{\tilde{\nu}}$ is that between the photon and the sneutrino. Furthermore, in case of a storage ring, ϕ_γ is the angle between the electron-photon plane and the plane of the e^+e^- orbits and $\phi_{\tilde{\nu}}$ is that between the electron-photon plane and the photon-sneutrino plane. (To be precise, the normal to the electron-photon plane is chosen parallel to $\mathbf{p}\times\mathbf{k}$, that of the photon-sneutrino plane is parallel to $\mathbf{k}\times\mathbf{k}_1$ and that of the plane of the e^+e^- orbits of a storage ring is chosen antiparallel to the direction of the magnetic field.) For the photon and sneutrino energy we use the variables $x=E_\gamma/E$ and $z=E_{\tilde{\nu}}/E$, where E_γ, $E_{\tilde{\nu}}$ are the energies of the photon and of the sneutrino, and E is the beam energy. All quantities are in the e^+e^- center-of-mass frame.

The boundaries for the sneutrino energy are

$$z_{\min}=1-\frac{x}{2}\left[1+\left[1-\frac{m^2_{\tilde{\nu}}}{E^2(1-x)}\right]^{1/2}\right] , \quad (14)$$

$$z_{\max}=1-\frac{x}{2}\left[1-\left[1-\frac{m^2_{\tilde{\nu}}}{E^2(1-x)}\right]^{1/2}\right] , \quad (15)$$

and the maximal photon energy is

$$x_{\max}=1-\frac{m^2_{\tilde{\nu}}}{E^2} . \quad (16)$$

For the photon energy spectrum $d\sigma/dx$ we define longitudinal polarization asymmetries as

$$a_L(P_\parallel,P'_\parallel;x)=\frac{(d\sigma/dx)(P_\parallel,P'_\parallel)-(d\sigma/dx)(-P_\parallel,-P'_\parallel)}{(d\sigma/dx)(P_\parallel,P'_\parallel)+(d\sigma/dx)(-P_\parallel,-P'_\parallel)} , \quad (17)$$

which for one or both beams polarized satisfy the relation

$$a_L(x)\equiv a_L(P_\parallel=1,P'_\parallel=-1;x)=a_L(P_\parallel=1,P'_\parallel=0;x)=-a_L(P_\parallel=0,P'_\parallel=1;x) . \quad (18)$$

The longitudinal polarization asymmetries $A_L(P_\parallel,P'_\parallel)$ of the total cross section are defined analogously to Eq. (17) and satisfy a relation similar to Eq. (18).

Appearing only in the azimuthal photon distribution, effects of transverse polarization can be studied by comparing ϕ_γ distributions of transversely polarized and unpolarized beams [3] or through suitable moments of the ϕ_γ distribution for transversely polarized beams [7]. The photon energy spectrum $d\sigma/dx$ and angular distribution $d\sigma/d\cos\theta_\gamma$ as well as the total cross section discussed in our numerical calculations are, however, not influenced by transverse beam polarizations.

III. NUMERICAL ANALYSIS

A. Scenarios

The region in the (M,μ) plane where $m_{\tilde{\chi}^0_1}<m_{\tilde{\nu}}<m_{\tilde{\chi}^0_2}$ and $m_{\tilde{\nu}}<m_{\tilde{\chi}^+_1}$ so that only the invisible sneutrino decay $\tilde{\nu}\to\nu+\tilde{\chi}^0_1$ is allowed can be seen in Fig. 2 for $m_{\tilde{\nu}}=80$ GeV (150 GeV) and $\tan\beta=1.7$. If one makes use of the renormalization-group equations based on a minimal $N=1$ supergravity with a common scalar mass m_0 at the unification point, the sneutrino mass is related to the SUSY parameters by [15,16]

$$m_{\tilde{\nu}}^2 = m_0^2 + 0.79M^2 + 0.5m_Z^2 \cos 2\beta \ . \quad (19)$$

Thus, for a given sneutrino mass there exists a maximal value of M ($M \leq 103$ GeV for $m_{\tilde{\nu}}=80$ GeV, $\tan\beta=1.7$ and $M < 176$ GeV for $m_{\tilde{\nu}}=150$ GeV, $\tan\beta=1.7$) and the (M,μ) region where the sneutrino is invisible shrinks to the shaded domain in Fig. 2, which is obviously larger for

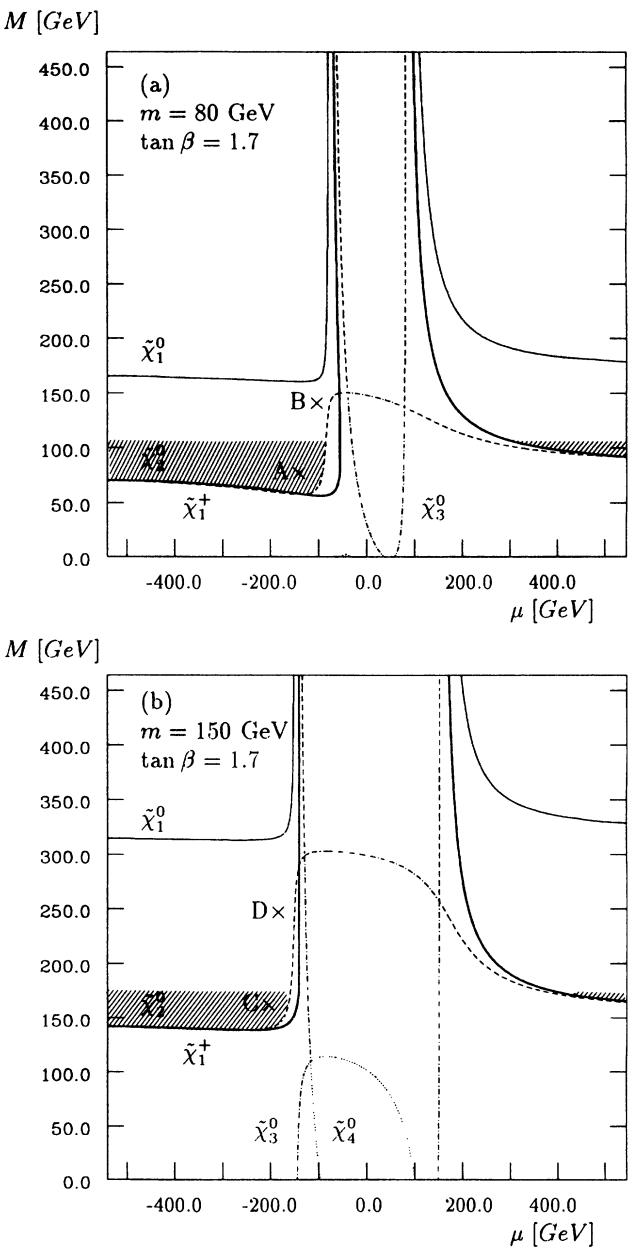

FIG. 2. Contour lines [(a) 80 GeV, (b) 150 GeV)] in the (M,μ) plane for the mass of the light chargino $\tilde{\chi}_1^+$ (thick solid line), the mass of the lightest neutralino $\tilde{\chi}_1^0$ (thin solid line), the second lightest neutralino $\tilde{\chi}_2^0$ (dashed line), the third lightest neutralino $\tilde{\chi}_3^0$ (dash-dotted line), and the heaviest neutralino $\tilde{\chi}_4^0$ (dotted line). In the domain between the contour line of $\tilde{\chi}_1^0$ and the upper one of the contour lines of $\tilde{\chi}_2^0$ and $\tilde{\chi}_1^+$ only the invisible decay $\tilde{\nu} \to \nu + \tilde{\chi}_1^0$ is possible. The mass relation Eq. (19) restricts this domain to the shaded region. The scenarios A–D of Table I are also indicated.

negative values of μ. Our scenarios A ($m_{\tilde{\nu}}=80$ GeV) and C ($m_{\tilde{\nu}}=150$ GeV) satisfy Eq. (19). Since the light chargino is essentially a W-ino in this parameter region, $\tilde{\chi}_1^+$ exchange is the dominating reaction mechanism for $\tilde{\nu}_e$ production for high energies far enough beyond the Z^0 region.

With regard to the supersymmetric background from radiative production of the lightest neutralino $e^+ + e^- \to \tilde{\chi}_1^0 + \tilde{\chi}_1^0 + \gamma$ one should note that in the parameter domain allowed by Eq. (19) the lightest neutralino is almost a pure photino.

One can escape these strong restrictions (see discussion in [16]) if one abandons Eq. (19). To study the effect of chargino mixing we will therefore also present numerical results for the somewhat "unorthodox" scenarios B ($m_{\tilde{\nu}}=80$ GeV) and D ($m_{\tilde{\nu}}=150$ GeV) where the light chargino is more Higgsino-like. In these scenarios, the lightest neutralino is a photino–Z-ino–Higgsino mixture, where the photino component, however, remains dominant.

Since in the relevant (M,μ) region the production cross sections depend only weakly on the sign of μ and on the value of β we present numerical results for $\mu<0$ and $\tan\beta=1.7$ only. Our scenarios A–D (see Table I) are compatible with the constraints for the allowed (M,μ) domain from lower bounds on the mass of the light chargino and that of the lightest neutralino from LEP experiments [14] and also with the bounds from UA2 [17] and the Collider Detector at Fermilab (CDF) [18] collaborations on the gluino mass. For illustration we show in Fig. 2 the position of our scenarios in the supersymmetric parameter space.

B. Cross sections and asymmetries

The photon distributions and the total cross sections have been calculated with cuts $x \geq 0.2$ for the photon energy and $|\cos\theta_\gamma| \leq 0.9$ for the photon scattering angle, corresponding to transverse photon momenta $k_T \geq 0.087E$. For the Z^0 mass and width we use the values $m_Z=91.175$ GeV and $\Gamma_Z=2.487$ GeV, furthermore we set $\sin^2\theta_W=0.23$ [19].

We will give numerical results for electron sneutrinos $\tilde{\nu}_e$ only. Since we will not deal with azimuthal ϕ_γ distributions and since the cross sections vanish for two longitudinally polarized beams with equal helicities ($P_\parallel = P'_\parallel = \pm 1$), we merely have to consider the longitudinal polarization configurations $P_\parallel = -P'_\parallel = +1$ and $P_\parallel = -P'_\parallel = -1$.

We begin the discussion of our results with some general comments on the *total cross section* which also apply to sneutrino pair production $e^+ + e^- \to \tilde{\nu} + \bar{\tilde{\nu}}$. Comparison of the $\tilde{\nu}_e$ cross section for polarization $P_\parallel = -P'_\parallel = +1$ with that for $P_\parallel = -P'_\parallel = -1$ reveals the importance of chargino exchange which becomes more significant with increasing W-ino component of the light chargino and also with increasing energy. Since for high energies Z^0 exchange is suppressed, the cross sections for $P_\parallel = -P'_\parallel = +1$ are expected to be smaller than those for $P_\parallel = -P'_\parallel = -1$ or for unpolarized beams, and the polar-

TABLE I. Chargino mass eigenvalues $m_{\tilde{\chi}_j^+}$ $(j=1,2)$ and mixing parameters V_{ij} in four different scenarios. Also shown are the mass eigenvalues $m_{\tilde{\chi}_1^0}$ and $m_{\tilde{\chi}_2^0}$ of the lightest and second lightest neutralino as well as the components N_{1i} $(i=1,\ldots,4)$ of the lightest neutralino state in the basis $(-i\lambda_\gamma, -i\lambda_Z, \psi^1_{H_1}\cos\beta - \psi^2_{H_2}\sin\beta, \psi^1_{H_1}\sin\beta + \psi^2_{H_2}\cos\beta)$ of weak eigenstates. For details see [10,11,26].

	Scenario	A	B	C	D
	$m_{\tilde{\nu}}$ (GeV)	80	80	150	150
Parameters	M (GeV)	80	150	160	150
	μ (GeV)	−136.8	−100	−200	−180
	$\tan\beta$	1.7	1.7	1.7	1.7
Chargino masses	$m_{\tilde{\chi}_1^+}$ (GeV)	95.7	112.6	166.3	187.4
	$m_{\tilde{\chi}_2^+}$ (GeV)	169.6	180.6	225.3	269.4
Mixing parameters	$V_{11}=V_{22}$	0.986	0.585	0.973	0.426
	$V_{21}=-V_{12}$	0.166	0.811	0.232	0.905
Neutralino masses	$m_{\tilde{\chi}_1^0}$ (GeV)	42	75	80	121
	$m_{\tilde{\chi}_2^0}$ (GeV)	96	97	165	177
Mixing parameters	N_{11}	0.955	0.855	0.913	0.883
	N_{12}	−0.257	−0.354	−0.380	0.420
	N_{13}	−0.105	−0.085	−0.096	−0.074
	N_{14}	−0.094	−0.367	−0.102	−0.194

ization asymmetry will always be negative in the energy region considered here. Furthermore, the cross sections for a Higgsino-like light chargino (scenarios B and D) are smaller than those for a W-ino-like light chargino (scenarios A and C). For the polarization $P_\parallel = -P'_\parallel = +1$ only Z^0 exchange contributes, so that there is no difference between production of electron, muon, and tau sneutrinos. For unpolarized beams or for polarized beams with $P_\parallel = -P'_\parallel = -1$, however, the cross sections for $\tilde{\nu}_\mu$ and $\tilde{\nu}_\tau$ production are considerably smaller than those for $\tilde{\nu}_e$ production provided that all sneutrinos have the same mass.

Figure 3 shows the *energy dependence* of the *total cross sections* for unpolarized beams. The phase-space integration has been performed with the help of the subroutine QUAND of the International Mathematical and Scientific Library (IMSL) [20] in a FORTRAN program and the results have been checked with multidimensional Romberg and Monte Carlo integrations. The different scenarios show the general features discussed above. For $m_{\tilde{\nu}}=80$ GeV the total cross section reaches its maximum at about 220-GeV beam energy, whereas for $m_{\tilde{\nu}}=150$ GeV it has reached only half its maximum at this energy and is still increasing beyond the energy region considered. For high energies ($E>250$ GeV for $m_{\tilde{\nu}}=80$ GeV, $E>300$ GeV for $m_{\tilde{\nu}}=150$ GeV) the cross section varies only smoothly with energy.

In Fig. 4, the *polarization asymmetries* of the *total cross section* are given. The absolute value of the asymmetry is the larger the more W-ino-like the light chargino is, it is increasing with decreasing chargino mass on the one hand and increasing sneutrino mass on the other hand. Towards higher energies the influence of chargino mixing is more and more suppressed.

The *photon energy spectrum* for unpolarized beams (Figs. 5–8) has been cut off at $x=0.2$ and extends to

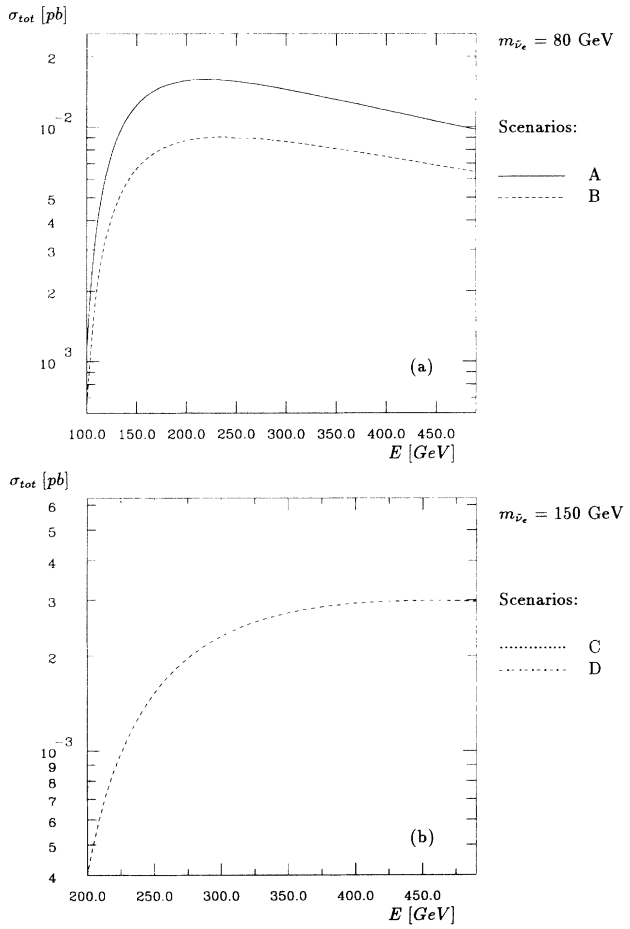

FIG. 3. Total cross section of $e^+e^- \to \tilde{\nu}_e\bar{\tilde{\nu}}_e\gamma$ for unpolarized beams in different chargino mixing scenarios; (a) for $m_{\tilde{\nu}_e}=80$ GeV, (b) for $m_{\tilde{\nu}_e}=150$ GeV. The solid line denotes scenario A, the dashed line scenario B, the dotted line scenario C, and the dash-dotted line scenario D.

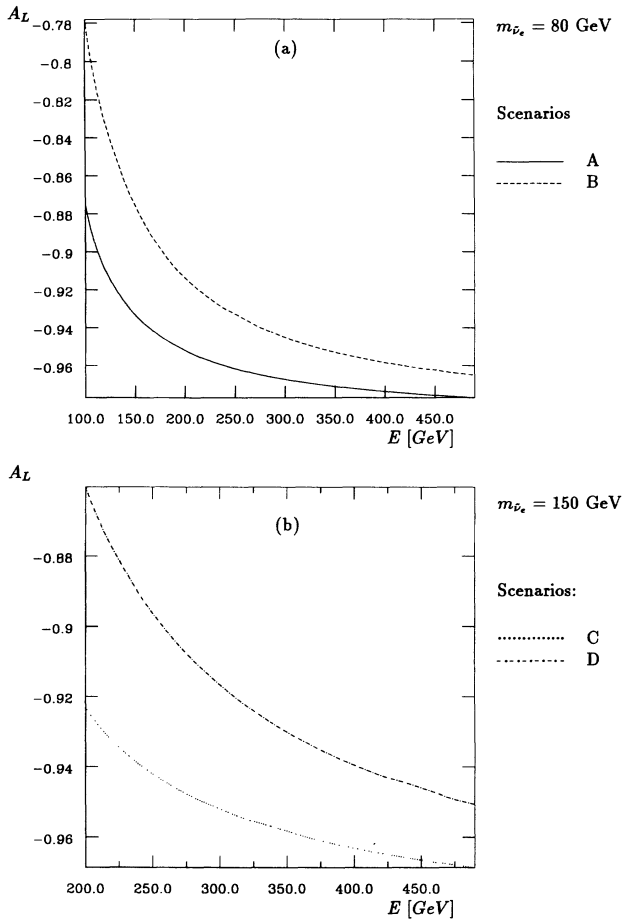

FIG. 4. Polarization asymmetry of the total cross section for $e^+e^- \to \tilde{\nu}_e\bar{\tilde{\nu}}_e\gamma$ in different chargino mixing scenarios; (a) for $m_{\tilde{\nu}_e} = 80$ GeV, (b) for $m_{\tilde{\nu}_e} = 150$ GeV. The solid line denotes scenario A, the dashed line scenario B, the dotted line scenario C and the dash-dotted line scenario D.

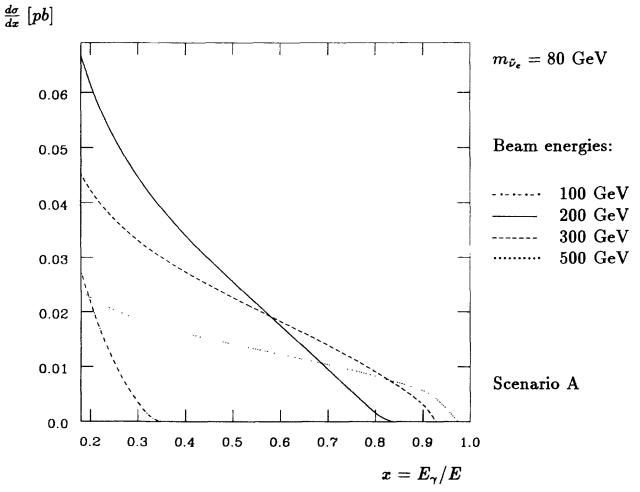

FIG. 5. Photon energy spectrum of $e^+e^- \to \tilde{\nu}_e\bar{\tilde{\nu}}_e\gamma$ for unpolarized beams and different energies in scenario A with $m_{\tilde{\nu}_e} = 80$ GeV. The dash-dotted line denotes $E = 100$ GeV, the solid line $E = 200$ GeV, the dashed line $E = 300$ GeV, and the dotted line $E = 500$ GeV.

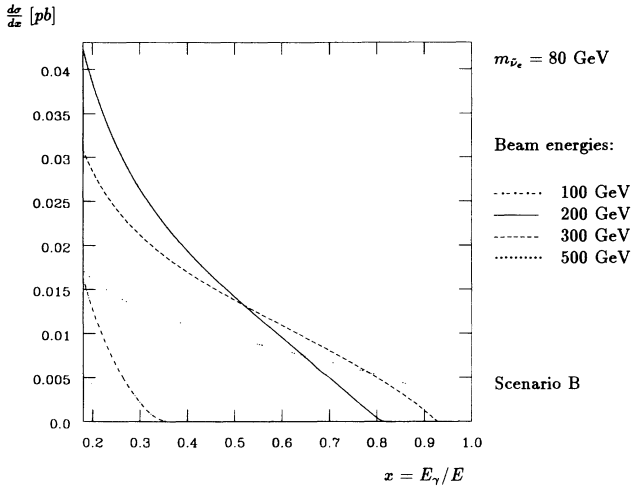

FIG. 6. Photon energy spectrum of $e^+e^- \to \tilde{\nu}_e\bar{\tilde{\nu}}_e\gamma$ for unpolarized beams and different energies in scenario B with $m_{\tilde{\nu}_e} = 80$ GeV. The dash-dotted line denotes $E = 100$ GeV, the solid line $E = 200$ GeV, the dashed line $E = 300$ GeV, and the dotted line $E = 500$ GeV.

$x_{\max} = 1 - m_{\tilde{\nu}}^2/E^2$ with the Z^0 peak far beyond this region. As for the absolute magnitude one recognizes the dependence on the nature of the charginos as already discussed for the total cross section. In the case of the lighter sneutrino ($m_{\tilde{\nu}} = 80$ GeV), the shape of the spectrum does not change much up to 200-GeV beam energy. Beyond 200 GeV, it flattens with increasing energy, so that for high beam energies the soft photon domain of the spectrum becomes suppressed. For the larger sneutrino mass ($m_{\tilde{\nu}} = 150$ GeV) this flattening occurs beyond about 300 GeV.

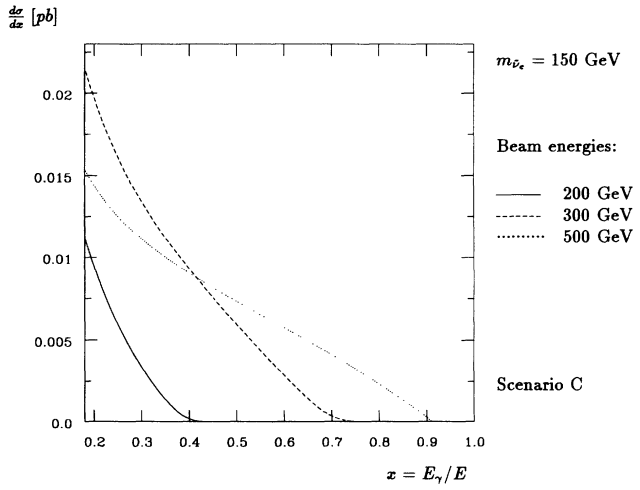

FIG. 7. Photon energy spectrum of $e^+e^- \to \tilde{\nu}_e\bar{\tilde{\nu}}_e\gamma$ for unpolarized beams and different energies in scenario C with $m_{\tilde{\nu}_e} = 150$ GeV. The solid line denotes $E = 200$ GeV, the dashed line $E = 300$ GeV, and the dotted line $E = 500$ GeV.

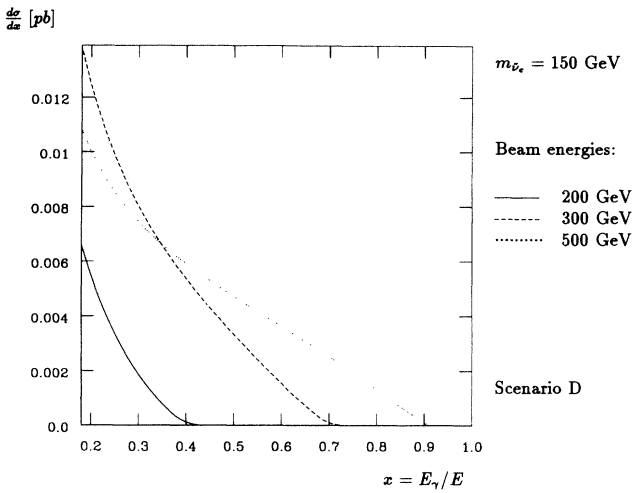

FIG. 8. Photon energy spectrum of $e^+e^- \to \tilde{\nu}_e\bar{\tilde{\nu}}_e\gamma$ for unpolarized beams and different energies in scenario D with $m_{\tilde{\nu}_e} = 150$ GeV. The solid line denotes $E = 200$ GeV, the dashed line $E = 300$ GeV, and the dotted line $E = 500$ GeV.

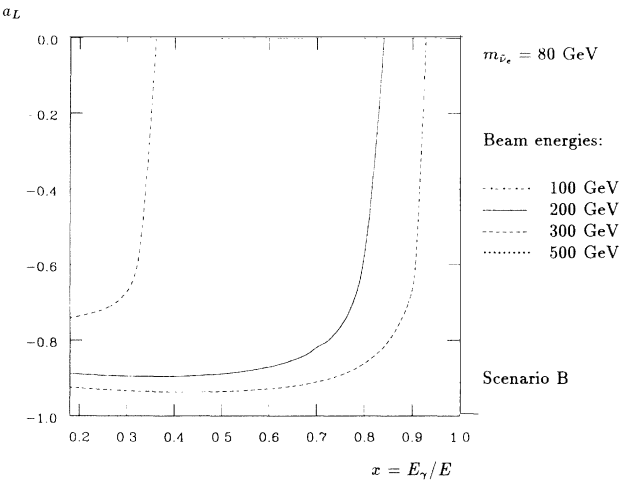

FIG. 10. Polarization asymmetry of the photon energy spectrum of $e^+e^- \to \tilde{\nu}_e\bar{\tilde{\nu}}_e\gamma$ for different energies in scenario B with $m_{\tilde{\nu}_e} = 80$ GeV. The dash-dotted line denotes $E = 100$ GeV, the solid line $E = 200$ GeV, the dashed line $E = 300$ GeV and the dotted line $E = 500$ GeV.

Figures 9–12 show the longitudinal *polarization asymmetry* of the *photon energy spectrum*. For beam energies higher than 200 GeV the asymmetries develop considerable values over most of the accessible x domain with a steep drop close by the upper boundary of the photon energy.

Since neither chargino mixing nor beam polarization changes the symmetrical shape of the photon angular distribution, we merely present as an example the angular distributions for unpolarized beams and longitudinal polarization $P_\parallel = -P'_\parallel = -1$ for scenario C with $m_{\tilde{\nu}} = 150$ GeV in Fig. 13. For all other scenarios, the distributions look very similar with the absolute magnitude showing the same systematic features as for the total cross section.

C. Background processes

The contributions to the background due to observable particles from the standard processes $e^+ + e^- \to e^+ + e^- + \gamma$, $\mu^+ + \mu^- + \gamma$, etc., can be exactly computed for the respective experimental setup [22] and will not be discussed here. The most important concurring supersym-

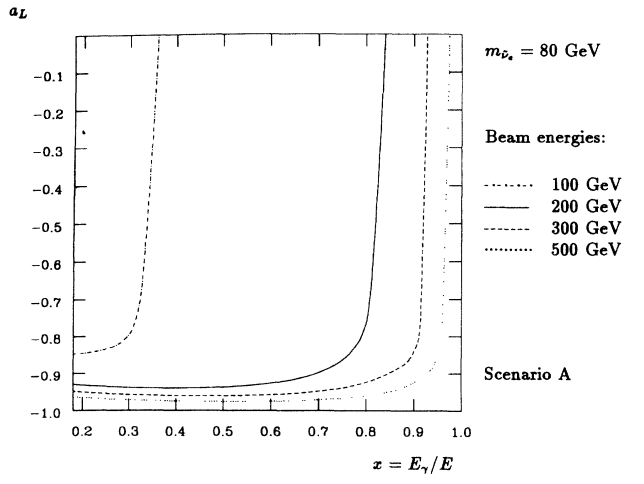

FIG. 9. Polarization asymmetry of the photon energy spectrum of $e^+e^- \to \tilde{\nu}_e\bar{\tilde{\nu}}_e\gamma$ for different energies in scenario A with $m_{\tilde{\nu}_e} = 80$ GeV. The dash-dotted line denotes $E = 100$ GeV, the solid line $E = 200$ GeV, the dashed line $E = 300$ GeV, and the dotted line $E = 500$ GeV.

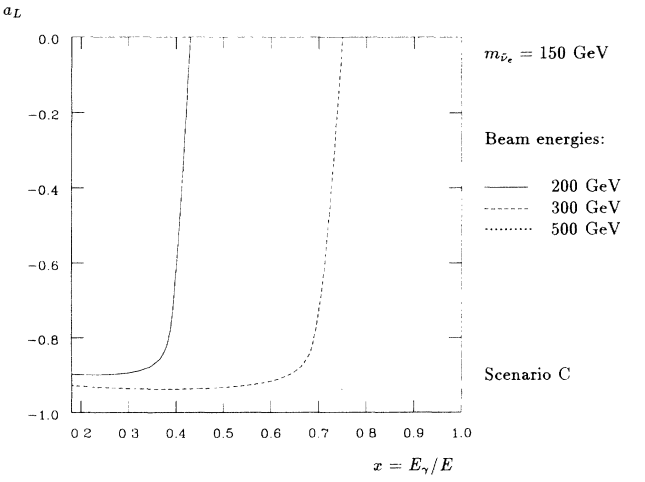

FIG. 11. Polarization asymmetry of the photon energy spectrum of $e^+e^- \to \tilde{\nu}_e\bar{\tilde{\nu}}_e\gamma$ for different energies in scenario C with $m_{\tilde{\nu}_e} = 150$ GeV. The solid line denotes $E = 200$ GeV, the dashed line $E = 300$ GeV, and the dotted line $E = 500$ GeV.

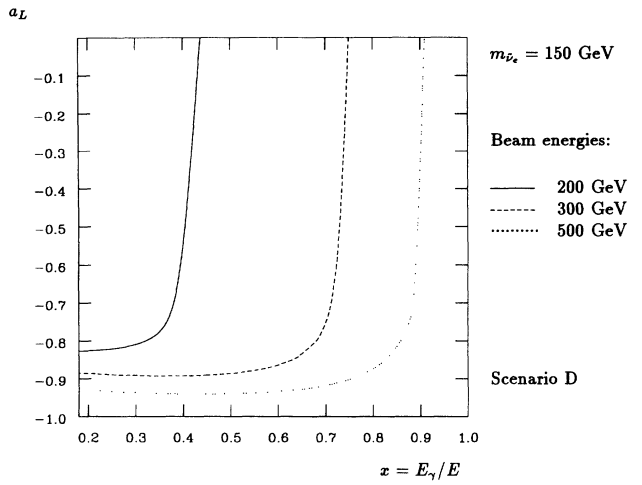

FIG. 12. Polarization asymmetry of the photon energy spectrum of $e^+e^- \to \tilde{\nu}_e\bar{\tilde{\nu}}_e\gamma$ for different energies in scenario D with $m_{\tilde{\nu}_e} = 150$ GeV. The solid line denotes $E = 200$ GeV, the dashed line $E = 300$ GeV, and the dotted line $E = 500$ GeV.

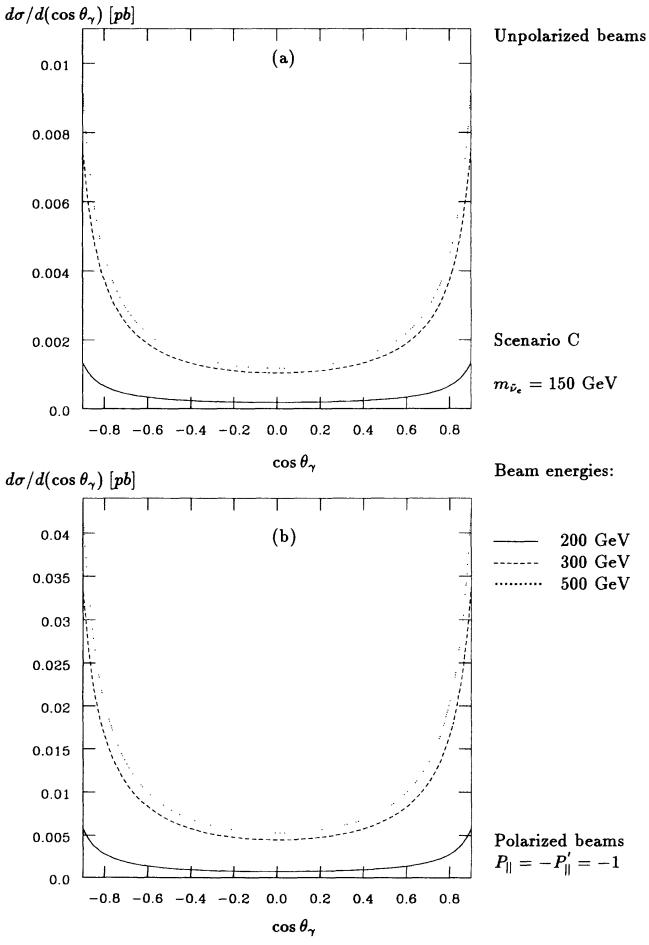

FIG. 13. Photon angular distribution of $e^+e^- \to \tilde{\nu}_e\bar{\tilde{\nu}}_e\gamma$ for different energies in scenario C with $m_{\tilde{\nu}_e} = 150$ GeV. The solid line denotes $E = 200$ GeV, the dashed line $E = 300$ GeV, and the dotted line $E = 500$ GeV.

metric process is the radiative production of the lightest neutralino $e^+ + e^- \to \tilde{\chi}_1^0 + \tilde{\chi}_1^0 + \gamma$. For similar scenarios, cross sections for this process are comparable to those for radiative sneutrino production [21]. The longitudinal polarization asymmetries, however, show drastic differences. As pointed out, the lightest neutralino is in scenarios A and C almost a pure photino and also in scenarios B and D the photino component is by far dominating, so that in the energy region considered here the longitudinal polarization asymmetries for $e^+ + e^- \to \tilde{\chi}_1^0 + \tilde{\chi}_1^0 + \gamma$ are positive [21] whereas they are negative for radiative sneutrino production (Figs. 4 and 9–12). This is consistent with the results of Chiappetta *et al.* [7] and allows discrimination between these two supersymmetric processes.

The most important background, however, comes from radiative neutrino production $e^+ + e^- \to \nu + \bar{\nu} + \gamma$. Using the helicity amplitudes given by Berends *et al.* [23], we have calculated for the energy region between 100 and 500 GeV the total cross section for unpolarized and polarized beams and the polarization asymmetries. (Because of the approximations involved the expression for the cross section given in [23] does not apply to the energy region considered here.)

Besides the lower cut at $x_{\min} = 0.2$ as before, the photon spectrum has also been cut off at $x_{\max} = 1 - m_{\tilde{\nu}}^2/E^2$ with $m_{\tilde{\nu}} = 80$ GeV, which corresponds to the maximum energy of photons produced in the process $e^+ + e^- \to \tilde{\nu} + \bar{\tilde{\nu}} + \gamma$.

Figure 14 shows for three neutrino generations the total cross section for unpolarized beams and for the polarization $P_\parallel = -P'_\parallel = -1$. By comparison with Fig. 3 one can see that for all our chargino mixing scenarios the total cross sections for production of 80-GeV sneutrinos with unpolarized beams are of the order of 5% or less of that for neutrino production (scenario A: 4.7% for

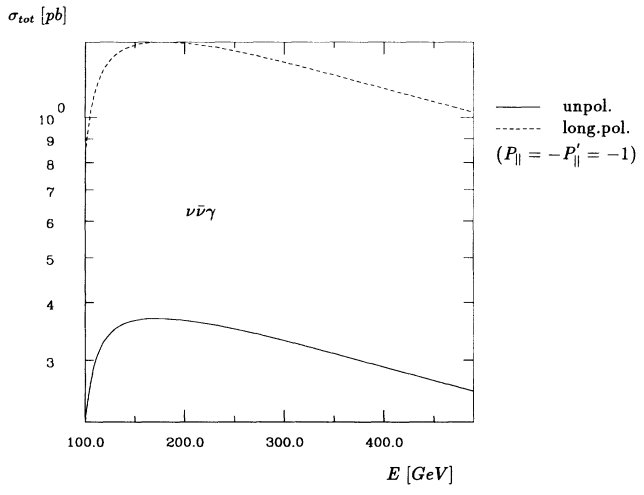

FIG. 14. Total cross section of $e^+e^- \to \nu\bar{\nu}\gamma$ for three neutrino generations with a cut of the photon energy at $x_{\max} = E_{\gamma_{\max}}/E = 1 - (80\text{ GeV})^2/E^2$. The solid line denotes unpolarized beams, the dashed line longitudinal polarized beams with $P_\parallel = -P'_\parallel = -1$.

$E=300$ GeV, 4.0% for $E>300$ GeV; scenario B: 2.5% for $E=300-500$ GeV; and still smaller for scenarios C and D). The situation is similar for polarized beams with $P_{\|}=-P'_{\|}=-1$, whereas for polarized beams with $P_{\|}=-P'_{\|}=+1$ the signal-to-background ratio is somewhat improved (Fig. 15). In this case, all cross sections are considerably smaller, that for sneutrino production reaches, however, about 10% of the neutrino cross section independent of chargino mixing, since now only Z^0 exchange contributes. One should notice that the neutrino cross sections have been calculated for three neutrino generations, whereas those of the supersymmetric process take into account electron sneutrino production only. Since for the polarization $P_{\|}=-P'_{\|}=+1$ the cross sections for production of $\tilde{\nu}_\mu$ and $\tilde{\nu}_\tau$ are identical to that for $\tilde{\nu}_e$ production (assuming mass degeneration of the three sneutrino generations), the signal from all three sneutrino generations would amount to 30% to the neutrino background. Vice versa, for this polarization configuration, radiative sneutrino production would be a considerable background for neutrino counting experiments.

For an integrated luminosity $\int \mathcal{L}dt=1.56\times10^4$ pb^{-1} corresponding to a 6-month running period with $\mathcal{L}=10^{33}$ cm^{-2} s^{-1} [24] at a 500-GeV e^+e^- linear collider, the statistical error for the unpolarized total cross section is between 1.3% ($E=200$ GeV) and 1.6% ($E=500$ GeV). Comparing this with the signal-to-background ratio of 4.7% and less we conclude that it would be at least rather difficult to observe a statistically significant deviation in the unpolarized cross section.

Although for polarized beams with $P_{\|}=-P'_{\|}=+1$ the signal from $\tilde{\nu}_e$ production amounts to 10% of the neutrino background the situation is still worse since for the same integrated luminosity the considerably reduced cross section entail large statistical errors between 6% ($E=200$ GeV) and 12% ($E=500$ GeV). Even for the rather optimistic assumption of three mass degenerated sneutrino generations with an improved signal-to-background ratio of 30% the use of polarized beams would have no advantage compared to experiments with unpolarized beams.

Figure 16 compares the longitudinal asymmetries of the total cross sections for scenarios A and B ($m_{\tilde{\nu}}=80$ GeV) with that for neutrino production. The difference between the asymmetries of the supersymmetric and the standard process is generally rather small. It is largest for a Higgsino-like chargino (scenario B) at "low" energies (approximately 15% for $E=100$ GeV and 5% for $E=250$ GeV). The difference is the smaller the more W-ino-like the chargino is, and it is further reduced with decreasing chargino mass. For high energies, the asymmetries become more and more model independent, approaching the value $A_L=-1$.

Since, however, the cross sections for neutrino production are at least 1 order of magnitude larger than those for the supersymmetric process, the polarization asymmetry of the total rate of one-photon events will be dominated by that of the background process. Thus, a difference of 10% between the asymmetries of the total cross sections for sneutrino and neutrino production appears as an effect of the order of 1% or less in the total number of one-photon events. This will be further reduced by assuming realistic values for the beam polarization between 30 and 50 %.

The discussed features of the total cross section are reflected by the photon energy spectrum. Figure 17 shows the photon spectrum for neutrino production with unpolarized beams with the significant resonance peak at $x_Z=1-m_Z^2/4E^2$, which for the sneutrino process lies outside the accessible x region with $x_{\max}=1-m_{\tilde{\nu}}^2/E^2$.

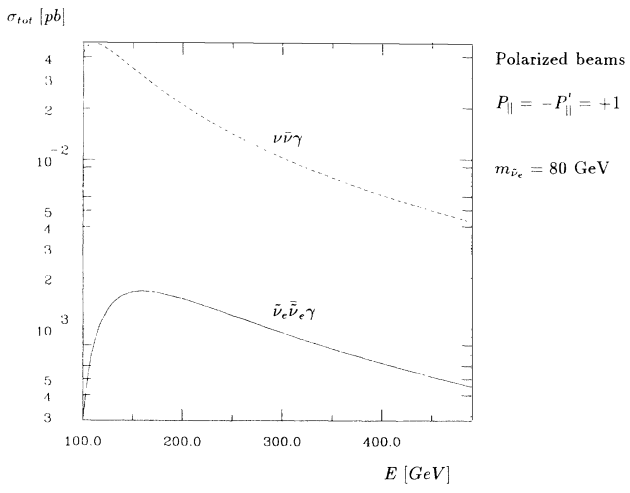

FIG. 15. Total cross section of $e^+e^-\to\tilde{\nu}_e\bar{\tilde{\nu}}_e\gamma$ with $m_{\tilde{\nu}_e}=80$ GeV and $e^+e^-\to\nu\bar{\nu}\gamma$ with three neutrino generations for polarized beams $P_{\|}=-P'_{\|}=+1$. For the process $e^+e^-\to\nu\bar{\nu}\gamma$ the photon energy has been cut off at $x_{\max}=E_{\gamma_{\max}}/E=1-(80\ \text{GeV})^2/E^2$.

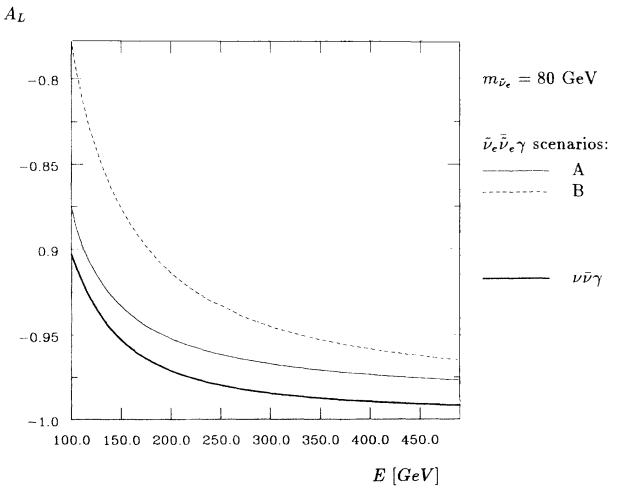

FIG. 16. Polarization asymmetries of the total cross sections of $e^+e^-\to\tilde{\nu}_e\bar{\tilde{\nu}}_e\gamma$ for $m_{\tilde{\nu}_e}=80$ GeV in scenario A (thin solid line) and scenario B (dashed line) and of $e^+e^-\to\nu\bar{\nu}\gamma$ for three neutrino generations with a cutoff in the photon energy at $x_{\max}=E_{\gamma_{\max}}/E=1-(80\ \text{GeV})^2/E^2$ (thick line).

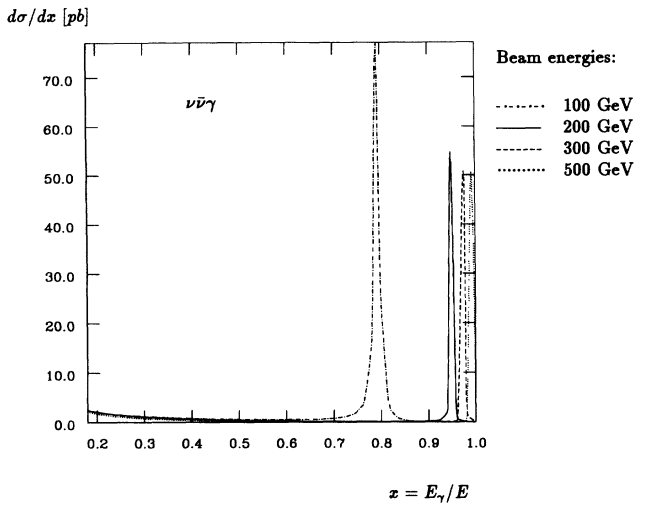

FIG. 17. Photon energy spectrum of $e^+e^- \to \nu\bar{\nu}\gamma$ with three neutrino generations for unpolarized beams and different energies. The dash-dotted line denotes $E = 100$ GeV, the solid line $E = 200$ GeV, the dashed line $E = 300$ GeV, and the dotted line $E = 500$ GeV.

For polarized beams with $P_\parallel = -P'_\parallel = -1$ the neutrino spectrum looks very similar with rates still 2–3 times higher. For both these cases the supersymmetric signal (Figs. 5–8) reaches at best about a few percent of that for neutrino production. Again the situation is different for the complementary longitudinal polarization $P_\parallel = -P'_\parallel = +1$ (Fig. 18), where the supersymmetric photon energy distribution reaches between 20 and 30% of that of the standard process.

Comparing the longitudinal polarization asymmetries of the photon spectrum for sneutrino production (Figs. 9–12) with those for the sneutrino background (Fig. 19) significant differences show up near the upper end $x_{\max}$ of the spectrum $[a_L(\tilde{\nu}\bar{\tilde{\nu}}\gamma) \approx -0.55$ in scenario B and $a_L(\nu\bar{\nu}\gamma) \approx -0.85$ for $E = 200$ GeV and $x = 0.8]$. But since in this region the sneutrino cross sections are rapidly decreasing, this difference is completely suppressed in the asymmetry of the photon rate. The situation is similar at the lower end of the photon spectrum. Here the differential cross section for sneutrino production is the largest, the difference of the asymmetries, however, is very small.

To summarize we conclude that due to the large irreducible background from $e^+ + e^- \to \nu + \bar{\nu} + \gamma$ it would be very difficult to identify a sneutrino which is lighter than both the light chargino and the second lightest neutralino. For unpolarized beams the signal would be less than approximately 5% of the background in our scenarios so that the observation of a statistically significant deviation in the cross section would be a difficult task. Because of the rather small differences between the cross-section asymmetries of the supersymmetric process and of the dominating standard background beam polarization cannot help identifying a sneutrino in the considered mass region.

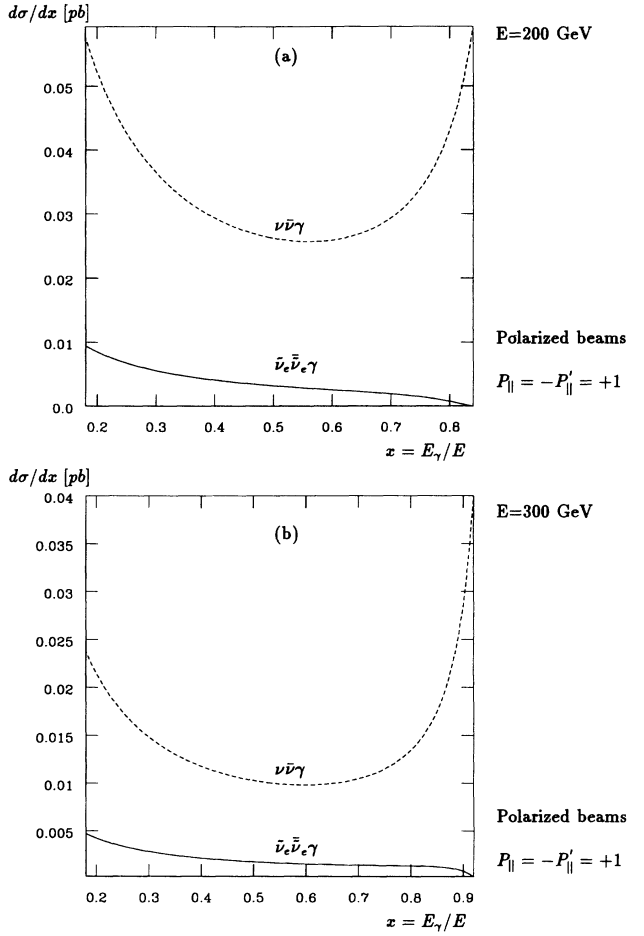

FIG. 18. Photon energy spectrum of $e^+e^- \to \tilde{\nu}_e\bar{\tilde{\nu}}_e\gamma$ with $m_{\tilde{\nu}_e} = 80$ GeV and of $e^+e^- \to \nu\bar{\nu}\gamma$ with three neutrino generations for polarized beams $P_\parallel = -P'_\parallel = +1$. (a) for $E = 200$ GeV, (b) for $E = 300$ GeV.

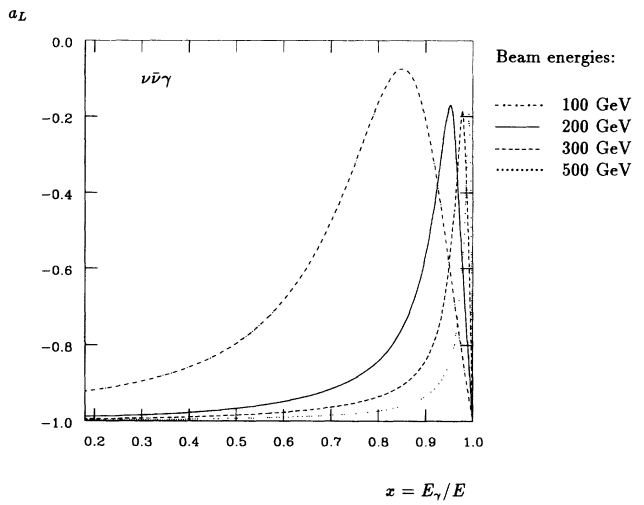

FIG. 19. Polarization asymmetry of the photon energy spectrum of $e^+e^- \to \nu\bar{\nu}\gamma$ with three neutrino generations for different energies. The dash-dotted line denotes $E = 100$ GeV, the solid line $E = 200$ GeV, the dashed line $E = 300$ GeV, and the dotted line $E = 500$ GeV.

ACKNOWLEDGMENTS

All numerical calculations were performed at the "Rechenzentrum der Universität Würzburg." H.F. was supported by "Bundesministerium für Forschung und Technologie" (BMFT), Bonn, Germany, Förderungskennzeichen 055WU91P2.

APPENDIX

We give a brief summary our notation and conventions for the description of beam polarization (see [25] for details) and list the explicit expressions for the coefficients X_s, X_t, X_{st}, X_s', and X_{st}' defined in Eq. (11).

The covariant density matrix for electrons with four-momentum p^μ and the polarization four-vector

$$\xi^\mu = \left(P^3 \frac{|\mathbf{p}|}{m_e}, P^1, P^2, P^3 \frac{E}{m_e} \right) \tag{A1}$$

is

$$\rho(p,\xi) = \tfrac{1}{2}(\not{p} + m_e)(1+\gamma^5 \not{\xi}) \ . \tag{A2}$$

In Eq. (A1) the z axis of the coordinate system is chosen along the direction of $\mathbf{p}$, so that $P^3 = P_\parallel$ is the longitudinal polarization, and P^1, P^2 are the components of transverse polarization.

In the high-energy limit ($E \gg m_e$), the polarization vector can be approximated by

$$\xi^\mu \approx P_\parallel \frac{p^\mu}{m_e} + P_\perp \tau^\mu \tag{A3}$$

with $\tau^\mu = (0, \tau^1, \tau^2, 0)$. The unit vector $\tau = (\tau^1, \tau^2, 0)$ characterizes the direction of transverse polarization. Then for the density matrix one obtains

$$\rho(p, P_\parallel, P_\perp) \approx \tfrac{1}{2}[(1+\gamma^5 P_\parallel)\not{p} - \gamma^5 P_\perp \not{p} \not{\tau}] \ . \tag{A4}$$

Similarly, for positrons with four-momentum p'^μ and polarization four-vector

$$\xi'^\mu = \left(-P'^3 \frac{|\mathbf{p}'|}{m_e}, P'^1, P'^2, -P'^3 \frac{E'}{m_e} \right) , \tag{A5}$$

the covariant density matrix

$$\rho'(p', \xi') = \tfrac{1}{2}(\not{p}' - m_e)(1+\gamma^5 \not{\xi}') \tag{A6}$$

can be approximated in the high-energy domain by

$$\rho'(p', P_\parallel', P_\perp') \approx \tfrac{1}{2}[(1-\gamma^5 P_\parallel')\not{p}' - \gamma^5 P_\perp' \not{p}' \not{\tau}'] \tag{A7}$$

with $\tau'^\mu = (0, \tau'^1, \tau'^2, 0)$. Again, the unit vector $\tau' = (\tau'^1, \tau'^2, 0)$ characterizes the direction of transverse positron polarization.

Subsequently choosing $\tau = \tau'$ we assume that the transverse polarization is parallel ($P_\perp, P_\perp' > 0$) or antiparallel ($P_\perp P_\perp' < 0$) but otherwise arbitrary. For the case of a storage ring, the azimuthal angle ϕ_γ between the electron-photon plane and the plane of the e^+e^- orbits is defined such that the direction of the natural transverse polarization is characterized by $\tau = (0,1,0)$ with $P_\perp > 0$ for electrons and $P_\perp' < 0$ for positrons.

The phase-space integrations have been performed in a coordinate frame with the z axis parallel to the photon three-momentum. For clearness, we add the expressions for the four-momenta and the transverse polarization four-vector in this frame:

$$k = E_\gamma \begin{pmatrix} 1 \\ 0 \\ 0 \\ 1 \end{pmatrix} , \quad k_1 = \begin{pmatrix} E_1 \\ \sqrt{E_1^2 - m_{\tilde{\nu}}^2}\ \sin\theta_{\tilde{\nu}} \cos(\phi_{\tilde{\nu}} + \phi_\gamma) \\ \sqrt{E_1^2 - m_{\tilde{\nu}}^2}\ \sin\theta_{\tilde{\nu}} \sin(\phi_{\tilde{\nu}} + \phi_\gamma) \\ \sqrt{E_1^2 - M_{\tilde{\nu}}^2}\ \cos\theta_{\tilde{\nu}} \end{pmatrix} ,$$

$$p_1 = \begin{pmatrix} E \\ E\sin\theta_\gamma \cos\phi_\gamma \\ E\sin\theta_\gamma \sin\phi_\gamma \\ E\cos\theta_\gamma \end{pmatrix} , \quad p_2 = \begin{pmatrix} E \\ -E\sin\theta_\gamma \cos\phi_\gamma \\ -E\sin\theta_\gamma \sin\phi_\gamma \\ -E\cos\theta_\gamma \end{pmatrix} , \tag{A8}$$

$$\xi_\perp = P_\perp \begin{pmatrix} 0 \\ -(1-\cos\theta_\gamma)\sin\phi_\gamma \cos\phi_\gamma \\ \cos\theta_\gamma + (1-\cos\theta_\gamma)\cos^2\phi_\gamma \\ -\sin\theta_\gamma \sin\phi_\gamma \end{pmatrix} .$$

Using the density matrices (A4) and (A7), we have calculated the coefficients X_s, etc., defined in Eq. (11), with the help of the program FEYNCALC [12]. The contributions of the Feynman amplitudes $\mathcal{M}_i$ and $\mathcal{M}_j$ [Eqs. (6)–(10)] will be denoted by $\mathcal{T}_{ij}$ for unpolarized and longitudinal polarized beams and by $\mathcal{T}_{ij}'$ for transverse polarization. Note that in Eq. (11) the degrees of polarization $P_\parallel$, $P_\parallel'$, $P_\perp$, and $P_\perp'$ have been factored out.

Using the notation

$$Z = (k_1+k_2)^2 - m_Z^2 + i m_Z \Gamma_Z \ , \tag{A9}$$

$$C_j = (k_1 - p_1)^2 - m_{\tilde{\chi}_j^+}^2 \ , \tag{A10}$$

$$C_j' = (k_2 - p_2)^2 - m_{\tilde{\chi}_j^+}^2 \ , \tag{A11}$$

$$\varepsilon(a,b,c,d) = \varepsilon^{\mu\nu\rho\sigma} a_\mu b_\nu c_\rho d_\sigma \ , \tag{A12}$$

with $\varepsilon^{0123} = 1$, we obtain for the contributions from Z^0 exchange, chargino exchange, and interference terms the expressions

$$X_s = \mathcal{T}_{44} + \mathcal{T}_{55} + \mathcal{T}_{45} \tag{A13}$$

with

$$\mathcal{T}_{44} = \frac{e^2 g^4}{4\cos^2\theta_W |Z|^2 (kp_1)} [(kp_2)(k_1k_2 - m_{\tilde{\nu}}^2) + (kk_1 - kk_2)(k_1p_2 - k_2p_2)] \ , \tag{A14}$$

$$\mathcal{T}_{55} = \mathcal{T}_{44}(p_1 \leftrightarrow p_2) \ , \tag{A15}$$

$$\mathcal{T}_{45}=\frac{e^2g^4}{4\cos^2\theta_W|Z|^2(kp_1)(kp_2)}\{(p_1p_2)[(k_1p_1-k_2p_1)(k_2p_1-k_1p_1)+(k_1k_2-m_{\tilde{\nu}}^2)(p_1p_2-2kp_1)]$$
$$+(kp_1)(k_1p_2-k_2p_2)(k_1p_2-k_2p_2+k_2p_1-k_1p_1)+(p_1\leftrightarrow p_2)\}\ , \tag{A16}$$

$$X_t=\mathcal{T}_{11}+\mathcal{T}_{22}+\mathcal{T}_{33}+\mathcal{T}_{12}+\mathcal{T}_{13}+\mathcal{T}_{23}\ , \tag{A17}$$

with

$$\mathcal{T}_{11}=\frac{e^2g^4}{2(kp_1)}\left[\sum_{j=1}^{2}\frac{|V_{j1}|^2}{C_j'}\right]^2[2(kk_2)(k_2p_2)-m_{\tilde{\nu}}^2(kp_2)]\ , \tag{A18}$$

$$\mathcal{T}_{22}=\mathcal{T}_{11}(p_1\leftrightarrow p_2,k_1\leftrightarrow k_2)\ , \tag{A19}$$

$$\mathcal{T}_{33}=e^2g^4\left[\frac{|V_{11}|^2|V_{21}|^2}{C_1C_1'C_2C_2'}16(k_1p_1)(k_2p_2)(m_{\tilde{\chi}_1^+}^2+m_{\tilde{\chi}_2^+}^2+2k_1k_2)+8(p_1p_2)(m_{\tilde{\chi}_1^+}^2m_{\tilde{\chi}_2^+}^2+m_{\tilde{\nu}}^4)\right.$$
$$\left.-16m_{\tilde{\nu}}^2[(k_1p_1)(k_1p_2)+(k_2p_1)(k_2p_2)]+\tfrac{1}{2}(V_{11}\rightarrow V_{21},m_{\tilde{\chi}_1^+}\rightarrow m_{\tilde{\chi}_2^+})+\tfrac{1}{2}(V_{21}\rightarrow V_{11},m_{\tilde{\chi}_2^+}\rightarrow m_{\tilde{\chi}_1^+})\right]\ , \tag{A20}$$

$$\mathcal{T}_{12}=\frac{e^2g^4}{(kp_1)(kp_2)}\left[\sum_{j=1}^{2}\frac{|V_{j1}|^2}{C_j'}\right]^2\{[(k_1k_2)(p_1p_2)-(k_1p_2)(k_2p_1)](p_1p_2-k_2p_1-k_1p_2)$$
$$-(k_1p_1)(k_2p_2)(p_1p_2+k_2p_1+k_1p_2)+m_{\tilde{\nu}}^2(p_1p_2)(k_1p_1+k_2p_1)\}\ , \tag{A21}$$

$$\mathcal{T}_{13}=\frac{e^2g^4}{kp_1}\sum_{j=1}^{2}\frac{|V_{j1}|^2}{C_j'}\sum_{i=1}^{2}\frac{|V_{i1}|^2}{C_i}\{2(k_1p_1)[2(k_2p_2)(kk_2-k_2p_1)+m_{\tilde{\nu}}^2(p_1p_2-kp_2)]$$
$$+m_{\tilde{\chi}_i^+}^2[(kp_1)(k_2p_2)+(kk_2)(p_1p_2)-(kp_2)(k_2p_1)]\}\ , \tag{A22}$$

$$\mathcal{T}_{23}=\mathcal{T}_{13}(p_1\leftrightarrow p_2,k_1\leftrightarrow k_2)\ , \tag{A23}$$

$$X_{st}=\mathcal{T}_{14}+\mathcal{T}_{15}+\mathcal{T}_{24}+\mathcal{T}_{25}+\mathcal{T}_{34}+\mathcal{T}_{35}\ , \tag{A24}$$

with

$$\mathcal{T}_{14}=\frac{e^2g^4}{2\cos^2\theta_W|Z|^2(kp_1)}\sum_{j=1}^{2}\frac{|V_{j1}|^2}{C_j'}\{\mathrm{Re}(Z)[(kp_2)(m_{\tilde{\nu}}^2-k_1k_2)+(kk_2)(k_1p_2-k_2p_2)+(k_2p_2)(kk_1-kk_2)]$$
$$-\mathrm{Im}(Z)\varepsilon(k,k_1,p_1,p_2)\}\ , \tag{A25}$$

$$\mathcal{T}_{15}=\frac{e^2g^4}{2\cos^2\theta_W|Z|^2(kp_1)(kp_2)}$$
$$\times\sum_{j=1}^{2}\frac{|V_{j1}|^2}{C_j'}[(\mathrm{Re}(Z)\{(p_1p_2)(m_{\tilde{\nu}}^2-k_1k_2)(p_1p_2-kp_1-kp_2)+(k_1p_1+k_2p_1)(k_2p_2-k_1p_2)(k_2p_2-k_2p_1)$$
$$+(k_2p_1-k_1p_1)[(p_1p_2)(kk_2)-(k_2p_1)(kp_2)]+(kp_2)(k_2p_1)(k_2p_2-k_1p_2)\}$$
$$-\mathrm{Im}(Z)\varepsilon(k,k_1,p_1,p_2)(k_1p_1+k_2p_2+kp_1-2k_2p_1))\ , \tag{A26}$$

$$\mathcal{T}_{24}=\mathcal{T}_{15}(p_1\leftrightarrow p_2,k_1\leftrightarrow k_2)\ , \tag{A27}$$

$$\mathcal{T}_{25}=\mathcal{T}_{14}(p_1\leftrightarrow p_2,k_1\leftrightarrow k_2)\ , \tag{A28}$$

$$\mathcal{T}_{34}=\frac{e^2g^4}{4\cos\theta_W|Z|^2(kp_1)}$$
$$\times\sum_{j=1}^{2}\frac{|V_{j1}|^2}{C_jC_j'}(\mathrm{Re}(Z)\{8(k_1p_1)[(k_1p_2)(k_1k_2-m_{\tilde{\nu}}^2)-(k_2p_2-k\quad k_2p_2-k_1k_2)]$$
$$+2m_{\tilde{\chi}_j^+}^2[(p_1p_2)(kk_1-kk_2)+(kp_1)(k_1p_2-k_2p_2)+(kp_2)(p_1k_2-p_1k_1)]\}$$
$$-4\,\mathrm{Im}(Z)m_{\tilde{\chi}_j^+}^2\varepsilon(k,k_1,p_1,p_2))\,, \tag{A29}$$

$$\mathcal{T}_{35}=\mathcal{T}_{34}(p_1\leftrightarrow p_2,k_1\leftrightarrow k_2)\,, \tag{A30}$$

$$X_s'=\mathcal{T}_{45}'$$
$$=\frac{e^2g^4}{2\cos^2\theta_W|Z|^2(kp_1)(kp_2)}$$
$$\times\{(kp_1)[(k_1p_2-k_2p_2)(kk_1-kk_2+k_1p_1-k_2p_1-k_1p_2+k_2p_2)$$
$$+(kp_2)(k_1k_2-m_{\tilde{\nu}}^2)-2m_{\tilde{\nu}}^2(p_1p_2)]$$
$$+(p_1p_2)[-\tfrac{1}{2}(kk_1-kk_2)^2+(\tau k)(\tau k_2-\tau k_1)(kk_1-kk_2-2k_1p_1+2k_2p_1)$$
$$+(\tau k_1-\tau k_2)^2(p_1p_2-2kp_1)+(\tau k)^2(m_{\tilde{\nu}}^2-k_1k_2)$$
$$+(kk_1)(2kp_1-p_1p_2)+(k_1p_2)(2k_2p_1-k_1p_1)-(k_2p_1)(k_2p_2)$$
$$+(kk_1-kk_2)(k_1p_1-k_2p_1)+m_{\tilde{\nu}}^2(p_1p_2)]+(p_1\leftrightarrow p_2)\}\,, \tag{A31}$$

$$X_{st}'=\mathcal{T}_{15}'+\mathcal{T}_{24}'+\mathcal{T}_{34}'+\mathcal{T}_{35}'\,, \tag{A32}$$

with

$$\mathcal{T}_{15}'=\frac{e^2g^4}{2\cos^2\theta_W|Z|^2(kp_1)(kp_2)}\frac{|V_{j1}|^2}{C_j'}$$
$$\times(\mathrm{Re}(Z)\{(kp_1)[(k_2p_2-k_1p_2)(k_2p_2-k_2p_1)+(kk_2)(k_1p_2-k_2p_2)+(kp_2)(m_{\tilde{\nu}}^2-k_1k_2)]$$
$$+(kp_2)(k_2p_1)(k_2p_1-k_2p_2-k_1p_1+k_1p_2+kk_1-kk_2)$$
$$+(p_1p_2)[(m_{\tilde{\nu}}^2-k_1k_2)(kp_1+kp_2-p_1p_2)+(k_2p_1)(k_2p_2-k_1p_2)$$
$$+(kk_2-k_2p_2)(kk_2-kk_1-k_2p_1+k_1p_1)]+2(\tau k_1)(\tau k_2)(p_1p_2)(p_1p_2-kp_1-kp_2)$$
$$+(\tau k)(\tau k_1)[(k_2p_2)(2p_1p_2-kp_1)+(kp_2)(k_2p_1)-(kk_2)(p_1p_2)]$$
$$+(\tau k)(\tau k_2)[(kp_1)(k_1p_2)-(kp_2)(k_1p_1)+(p_1p_2)(2kk_2-kk_1+2k_1p_1-2k_2p_1-2k_2p_2)]$$
$$+(\tau k)^2[(k_1p_1)(k_2p_2)-(k_1p_2)(k_2p_1)+(p_1p_2)(k_1k_2-m_{\tilde{\nu}}^2)]+2(\tau k_2)^2(p_1p_2)(kp_1+kp_2-p_1p_2)\}$$
$$+\mathrm{Im}(Z)\{\varepsilon(k,k_1,p_1,p_2)(kk_1-kk_2+k_2p_1-k_2p_2-k_1p_1+k_1p_2-2kp_1)$$
$$+\varepsilon(\tau,k,p_1,p_2)[(\tau k)(2p_1k_2+kk_1-2kp_1-2kk_2-2k_1p_1+k_1k_2-m_{\tilde{\nu}}^2)+4(\tau k_1)(kp_1)]$$
$$+\varepsilon(\tau,k_1,p_1,p_2)[(\tau k)(kk_1+2kp_1-3kk_2-2k_1p_1-2p_1p_2+2k_2p_1)+(\tau k_1)(4kp_1-4p_1p_2)]$$
$$-\varepsilon(\tau,k,k_1,p_1)(\tau k)(p_1p_2)-\varepsilon(\tau,k,k_1,p_2)(3\tau k+4\tau k_1)(p_1p_2)\})\,, \tag{A33}$$

$$\mathcal{T}_{24}'=\mathcal{T}_{15}'(p_1\leftrightarrow p_2,k_1\leftrightarrow k_2)\,, \tag{A34}$$

$$\mathcal{T}'_{34}=\frac{e^2g^4}{2\cos^2\theta_W(kp_1)}$$
$$\times\sum_{j=1}^{2}\frac{|V_{j1}|^2}{C_jC'_j}(\mathrm{Re}(Z)\{2(kk_1)[(k_2p_1)(k_2p_2)-(k_1p_1)(k_2p_2)-(k_1p_2)(k_2p_1)+(k_1k_2)(p_1p_2)]$$
$$+2(k_2p_2)[(kk_2)(k_1p_1)-(kp_1)(k_1k_2)+(k_1p_1)^2-2(k_1p_1)(k_2p_1)]$$
$$-2(k_1k_2)(k_1p_2)(p_1p_2)+2(k_1p_1)(k_1p_2)(k_2p_1)$$
$$+m_{\tilde{\nu}}^2[(kp_2)(k_2p_1-k_1p_1)+(kp_1)(k_1p_2+k_2p_2)+(p_1p_2)(2k_1p_1-kk_1-kk_2)]$$
$$+2(\tau k_2)^2[(kp_1)(k_1p_2)-(kp_2)(k_1p_1)+2(p_1p_2)(k_1p_1-kk_1)]$$
$$+2(\tau k_1)(\tau k_2)[(kp_1)(k_2p_1)-(kp_1)(k_2p_2)+(p_1p_2)(2kk_1-kk_2-2k_1p_1)]$$
$$+2(\tau k)(\tau k_2)[(k_1k_2)(p_1p_2)-(k_1p_2)(k_2p_1)+(k_1p_1)(k_2p_2)-m_{\tilde{\nu}}^2]\}$$
$$+\mathrm{Im}(Z)\{\varepsilon(k,k_1,p_1,p_2)(k_1k_2-k_2p_1-kk_1-kk_2+k_1p_1)$$
$$+\varepsilon(\tau,k,p_1,p_2)(\tau k_2)(kk_1-2k_1p_1+k_1k_2-m_{\tilde{\nu}}^2)$$
$$+\varepsilon(\tau,k_1,p_1,p_2)(\tau k_2)(3kk_1-kk_2-4k_1p_1)$$
$$-[\varepsilon(\tau,k,k_1,p_2)+\varepsilon(\tau,k,k_1,p_2)](\tau k_2)(p_1p_2)\}), \quad \text{(A35)}$$

$$\mathcal{T}'_{35}=\mathcal{T}'_{34}(p_1\leftrightarrow p_2)\ . \quad \text{(A36)}$$

[1] U. Amaldi, W. deBoer, and H. Fürstenau, Phys. Lett. B **260**, 447 (1991).

[2] P. Chiappetta, J. Soffer, P. Taxil, F. M. Renard, and P. Sorba, Nucl. Phys. **B259**, 365 (1984).

[3] M. Wendel and H. Fraas, Phys. Rev. D **44**, 60 (1991).

[4] H. Baer, A. Bartl, D. Karatas, W. Majerotto, and X. Tata, Int. J. Mod. Phys. A **4**, 4111 (1989).

[5] A. Bartl, H. Fraas, and W. Majerotto, Z. Phys. C **41**, 475 (1988).

[6] A. Bartl, M. Drees, W. Majerotto, and B. Mösslacher, in *Physics at HERA*, Proceedings of the Workshop, Hamburg, Germany, 1991, edited by W. Buchmüller and G. Ingelman (DESY, Hamburg, 1992), p. 1118.

[7] P. Chiappetta, J. Ph. Guillet, and F. M. Renard, Nucl. Phys. **B281**, 381 (1987).

[8] H. Baer, M. Drees, and X. Tata, Phys. Rev. D **41**, 3414 (1990).

[9] M. Chen, C. Dionisi, M. Martinez, and X. Tata, Phys. Rep. **159**, 201 (1988).

[10] H. E. Haber and G. L. Kane, Phys. Rep. **117**, 75 (1985).

[11] A. Bartl, H. Fraas, W. Majerotto, and B. Mösslacher, Z. Phys. C **55**, 257 (1992).

[12] R. Mertig, M. Böhm, and A. Denner, Comput. Phys. Commun. **64**, 345 (1991).

[13] B. de Wit and J. Smith, *Field Theory in Particle Physics* (North-Holland, Amsterdam, 1986).

[14] ALEPH Collaboration, D. Decamp *et al.*, Phys. Rep. **216**, 253 (1992).

[15] A. Bartl, W. Majerotto, and B. Mösslacher, in e^+e^- *Collisions at 500 GeV: The Physics Potential,* Proceedings of the Workshop, Munich, Annecy, Hamburg, Germany, 1991, edited by P. M. Zerwas (DESY Report No. 92-123B, Hamburg, 1992), p. 641.

[16] L. J. Hall and J. Polchinski, Phys. Lett. **152B**, 335 (1985).

[17] UA2 Collaboration, J. Alitti *et al.*, Phys. Lett. B **235**, 363 (1990).

[18] CDF Collaboration, F. Abe *et al.*, Phys. Rev. Lett. **69**, 3439 (1992).

[19] The LEP Collaborations: ALEPH, DELPHI, L3, and OPAL, Phys. Lett. B **276**, 247 (1992).

[20] IMSL MATH/LIBRARY version 1.0, User's Manual, 1987.

[21] M. Bayer and H. Fraas (unpublished).

[22] G. Barbiellini, B. Richter, and J. L. Siegrist, Phys. Lett. **106B**, 414 (1981); J. Bartels, A. Fridman, A. Schwarz, and T. T. Wu, Z. Phys. C **23**, 295 (1984); M. Caffo, R. Gatto, and E. Remiddi, Phys. Lett. B **173**, 91 (1986).

[23] F. A. Berends, G. J. H. Burgers, C. Mana, M. Martinez, and W. L. van Nerven, Nucl. Phys. **B301**, 583 (1988).

[24] P. M. Zerwas, in e^+e^- *Collisions at 500 GeV: The Physics Potential* [15], Vol. I.

[25] F. M. Renard, *Basics of Electron Positron Collisions* (Editions Frontières, Dreux, 1981).

[26] A. Bartl, H. Fraas, W. Majerotto, and N. Oshimo, Phys. Rev. D **40**, 1594 (1989).